Icarus 287 (2017) 152–160

Contents lists available at ScienceDirect

Icarus

journal homepage: www.elsevier.com/locate/icarus

Charon's light curves, as observed by New Horizons' Ralph color camera (MVIC) on approach to the Pluto system

C.J.A. Howett[a,*], K. Ennico[b], C.B. Olkin[a], M.W. Buie[a], A.J. Verbiscer[c], A.M. Zangari[a], A.H. Parker[a], D.C. Reuter[d], W.M. Grundy[e], H.A. Weaver[f], L.A. Young[a], S.A. Stern[a]

[a] Southwest Research Institute, Boulder, CO 80302, USA
[b] NASA Ames Research Center, Space Science Division, Moffett Field, CA 94035, USA
[c] Department of Astronomy, University of Virginia, Charlottesville, VA 22904, USA
[d] NASA Goddard Space Flight Center, Greenbelt, MD 20771, USA
[e] Lowell Observatory, Flagstaff, AZ 86001, USA
[f] Johns Hopkins University Applied Physics Laboratory, Laurel, MD 20723, USA

ARTICLE INFO

Article history:
Received 15 May 2016
Revised 10 August 2016
Accepted 20 September 2016
Available online 30 September 2016

Keywords:
Charon
Satellites, surfaces
Satellites, general

ABSTRACT

Light curves produced from color observations taken during New Horizons' approach to the Pluto-system by its Multi-spectral Visible Imaging Camera (MVIC, part of the Ralph instrument) are analyzed. Fifty seven observations were analyzed, they were obtained between 9th April and 3rd July 2015, at a phase angle of 14.5° to 15.1°, sub-observer latitude of 51.2 °N to 51.5 °N, and a sub-solar latitude of 41.2°N. MVIC has four color channels; all are discussed for completeness but only two were found to produce reliable light curves: Blue (400–550 nm) and Red (540–700 nm). The other two channels, Near Infrared (780–975 nm) and Methane-Band (860–910 nm), were found to be potentially erroneous and too noisy respectively. The Blue and Red light curves show that Charon's surface is neutral in color, but slightly brighter on its Pluto-facing hemisphere. This is consistent with previous studies made with the Johnson B and V bands, which are at shorter wavelengths than that of the MVIC Blue and Red channel respectively.

1. Introduction

1.1. Intro to New Horizons and the MVIC instrument

The New Horizons spacecraft launched on the 19th January 2006 bound for the Pluto-system. On the 14th July 2015 New Horizons reached closest approach, at a distance of 12,479 km and 28,824 km from Pluto's and Charon's surfaces respectively (Stern et al., 2015). However, New Horizons started observing the Pluto-system long before encounter and this paper discusses the results obtained during its approach by MVIC, the Multi-spectral Visible Imaging Camera, part of Ralph instrument. Reuter et al. (2008) provide full details of the instrument, so only an overview is given here for orientation.

MVIC has seven independent CCD arrays, held on a single substrate, read out using one of two independent redundant electronics (called side 0 and side 1). Six of these CCDs have 5024×32 pixels each, and operate in Time Delay and Integration mode (TDI). Four of the TDI arrays have a color filter, whilst the other two are panchromatic TDI with the same wavelength range for redundancy. The final array is a panchromatic frame transfer camera with a 5024×128 pixel array, primarily designed for optical navigation.

TDI is a way of building up large format image as the field of view (FOV) is scanned across a scene. It works by syncing the transfer rate between rows to the spacecraft's scan rate, thus the same scene passes through each of the rows before it is read out, effectively increasing the integration time. The frame transfer camera is operated in the more traditional stare mode.

The four color filters of MVIC are: Blue (400-550 nm), Red (540-700 nm), Near-Infrared (NIR, 780-975 nm) and Methane-Band (CH4, 860-910 nm). The Panchromatic TDI and frame transfer detectors are sensitive to the 400-975 nm bandpass. Howett et al. (2016) give the pivot wavelength of the four channels as: 492, 624, 861 and 883 nm for the Blue, Red, NIR and CH4 channels respectively. So comparing to historically used ground-based filters the pivot wavelength of both the MVIC Blue and Red channels are at longer wavelength than that of the Johnson B and V bands (442 and 540 nm).

1.2. Intro to previous Charon light curve observations

By solar-system exploration standards, Charon, Pluto's largest satellite was discovered remarkably recently (Christy and Harrington, 1978). However, since its discovery much work has been

* Corresponding author at: 1050 Walnut Street, Suite 300, Boulder, Colorado, 80302, USA. Fax: +1 303-546-9687.
E-mail address: howett@boulder.swri.edu (C.J.A. Howett).

http://dx.doi.org/10.1016/j.icarus.2016.09.031
0019-1035/

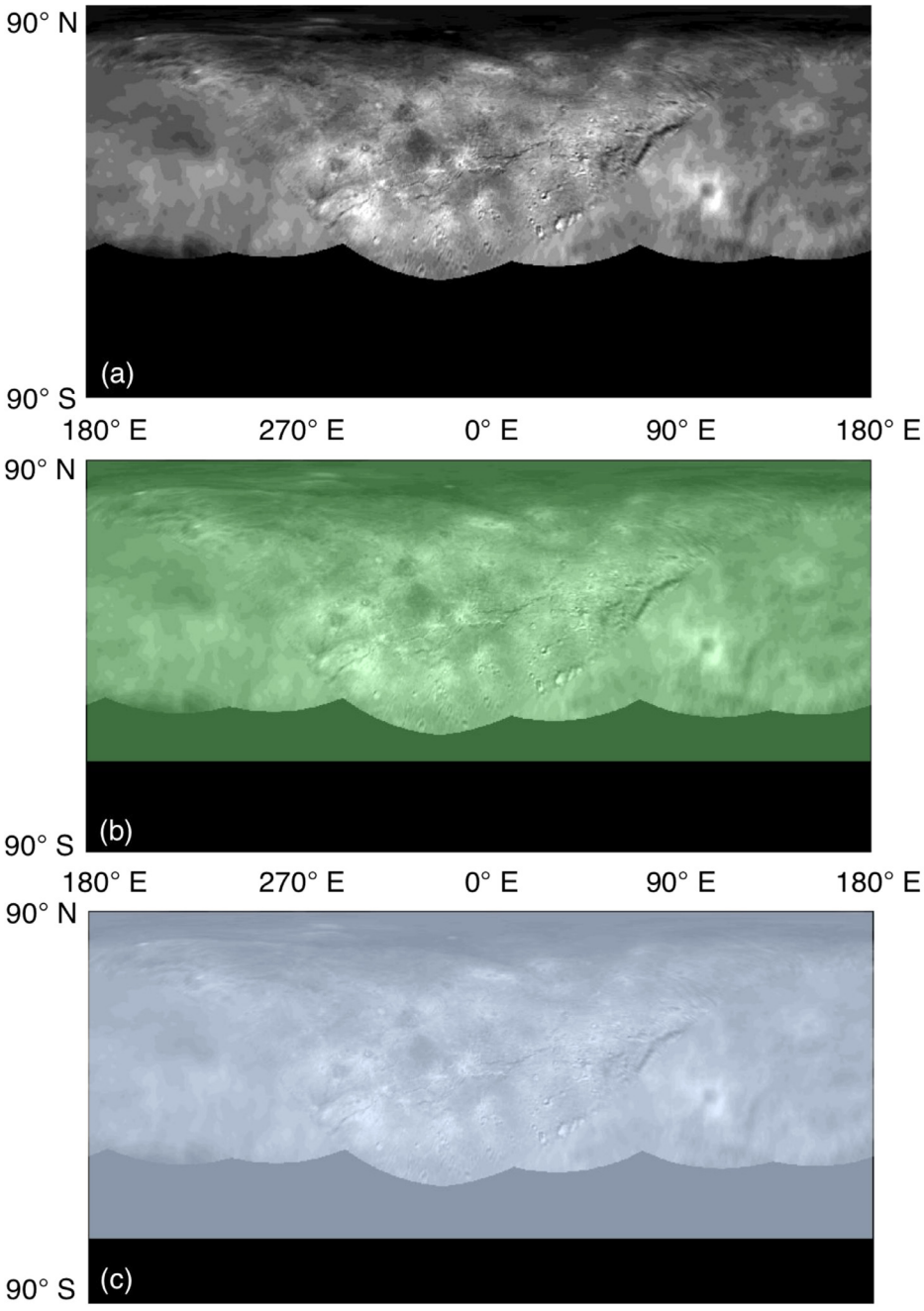

Fig. 1. (a) Charon base-map, a simple cylindrical mosaic of New Horizons' Horizons Long Range Reconnaissance Imager (LORRI) images. (b and c) the same base-map but with the area observed by MVIC shaded in green, and Buie et al. (2010) shaded in blue. Mordor Macula is the dark northern polar region (c.f. Stern et al., 2015). (For interpretation of the references to colour in this figure legend, the reader is referred to the web version of this article.)

undertaken to understand Charon. This effort was largely aided by a series of mutual events in the early- and mid-1980 s, which made it possible to understand the different characteristics of these two (previously impossible to separate) distant worlds. Excellent reviews on the body of mutual event results are available in the literature; for example see Binzel and Hubbard (1997) and Buie (1997a). Mutual event observations provided the first global surface properties for both Pluto and Charon, and the opportunity to begin monitoring their seasonal variations (although this is complicated by simultaneous changes in both the viewing geometry and solar illumination, for example see Hansen and Paige, 1996). For Charon the most important result was that its color, composition and albedo are different to that of Pluto. Specifically Charon has a neutral grey surface, compared to Pluto's redder one (Binzel, 1988; Reinsch et al., 1994) and Charon's surface is largely water ice compared to Pluto's largely nitrogen- and methane-ice surface (see references within Cruikshank et al., 1997). With a single scattering albedo (ω) between 0.03 and 0.98 Charon is darker than Pluto (ω of 0.2 to 0.98) (Buie et al. 1992; Stern et al. 2015). New Horizons resolved Charon's albedo features, discovering that its most prominent albedo feature was a dark northern polar spot (informally called Mordor Macula). This region, shown in Fig. 1, is ~275 km across and is about half as bright as the rest of Charon (Stern et al. 2015).

More recently telescope advances have made it possible to resolve Pluto and Charon, so their differences can be observed

without the need for rare mutual events. Arguably the most important advance for Charon light curve science was the commissioning of the Hubble-Space Telescope (HST). Buie et al. (1997b) used the Wide Field/Planetary Camera (WFPC1) to determine Charon's V magnitude light curve. Buie et al. (2010) improved upon this result using data taken with HST's Advanced Camera for Surveys High-resolution Camera (ACS) in 2002 and 2003 to determine the light curves of both Pluto and Charon. Both papers found that Charon's light curve varied by ~8% in magnitude, and Charon's anti-Pluto hemisphere is darker than its Pluto-facing one. Charon's solar phase at the time Buie et al. (2010) observed it varied from 0.3° and 1.7°, much lower than that observed by New Horizons on approach to the Pluto system (see Table 1). Furthermore the sub-observer latitude during Buie's observations varied from 28° to 32°, approximately 13° lower than the New Horizons observations. Bosh et al. (1992) showed Charon also displayed photometric variability in the infrared.

1.3. MVIC color observations of Charon

New Horizons officially began observing Pluto and Charon using Long Range Reconnaissance Imager (LORRI) during the

Table 1
Details of the observations used to make the Charon light curves, each observation was made with all of the color filters using the same exposure times and electronic sides. Mission Event Time (MET) is the number of seconds past 19th January 2006 18:08:02 UTC.

Mid-Time of Observation (UTC)	Mission Event Time (MET)	Exposure Time (s)	Range (km)	Electronic Side	Solar Phase Angle (°)	Sub-Spacecraft Longitude (°E)	Sub-Spacecraft Latitude (°)
2015-04-09T04:49:05.341	290,860,851	0.59	114,681,890	0	14.50	353.9	43.2
2015-04-12T03:12:05.344	291,114,231	0.59	111,192,010	1	14.51	188.6	43.2
2015-04-13T03:32:05.345	291,201,831	0.59	109,983,870	0	14.51	131.4	43.2
2015-04-13T21:48:05.346	291,267,591	0.59	109,076,280	1	14.52	88.5	43.2
2015-04-14T09:03:05.347	291,308,091	0.59	108,517,290	0	14.52	62.1	43.2
2015-04-15T03:22:05.348	291,374,031	0.59	107,607,580	1	14.53	19.1	43.2
2015-04-15T21:50:05.348	291,440,511	0.59	106,691,220	0	14.54	335.7	43.2
2015-04-16T09:08:05.349	291,481,191	0.59	106,130,890	1	14.55	309.2	43.2
2015-04-17T03:26:05.350	291,547,071	0.59	105,223,810	0	14.55	266.2	43.2
2015-04-17T20:36:05.350	291,608,871	0.59	104,372,850	1	14.55	225.9	43.2
2015-04-18T08:29:05.351	291,651,651	0.59	103,783,500	0	14.55	198.0	43.2
2015-04-20T07:45:05.353	291,821,811	0.60	101,436,210	1	14.55	86.9	43.2
2015-04-22T09:11:05.355	291,999,771	0.59	98,981,798	0	14.58	330.9	43.2
2015-04-25T02:12:05.358	292,233,831	0.60	95,758,152	1	14.58	178.2	43.2
2015-04-27T02:04:05.360	292,406,151	0.59	93,380,492	0	14.59	65.7	43.2
2015-04-28T17:02:05.362	292,546,431	0.59	91,446,028	1	14.62	334.2	43.2
2015-05-01T01:51:05.364	292,750,971	0.59	88,629,299	0	14.62	200.8	43.2
2015-05-03T01:33:35.366	292,922,721	0.59	86,260,199	1	14.62	88.7	43.2
2015-05-05T01:32:05.368	293,095,431	0.59	83,878,083	0	14.65	336.1	43.2
2015-05-08T06:38:05.371	293,372,991	0.59	80,055,007	1	14.65	155.0	43.2
2015-05-09T03:14:05.372	293,447,151	0.59	79,031,742	0	14.66	106.6	43.2
2015-05-09T20:04:05.373	293,507,751	0.60	78,195,338	1	14.66	67.1	43.2
2015-05-10T06:30:05.373	293,545,311	0.59	77,677,053	0	14.67	42.6	43.2
2015-05-11T00:18:05.374	293,609,391	0.59	76,793,343	1	14.68	0.8	43.2
2015-05-11T19:46:05.375	293,679,471	0.59	75,827,790	0	14.69	315.1	43.2
2015-05-12T07:44:05.376	293,722,551	0.59	75,234,599	1	14.70	287.0	43.2
2015-05-13T02:39:05.376	293,790,651	0.59	74,297,025	0	14.70	242.6	43.2
2015-05-13T19:31:35.377	293,851,401	0.59	73,460,297	1	14.69	202.9	43.2
2015-05-14T01:42:05.377	293,873,631	0.59	73,153,958	0	14.69	188.4	43.2
2015-05-14T19:45:05.378	293,938,611	0.60	72,257,950	1	14.69	146.0	43.2
2015-05-29T11:38:05.393	295,205,391	0.59	54,793,392	1	14.78	39.6	43.2
2015-05-29T18:34:05.394	295,230,351	0.59	54,449,111	0	14.79	23.3	43.2
2015-05-30T05:50:05.394	295,270,911	0.60	53,889,906	0	14.80	356.9	43.2
2015-05-31T01:21:05.395	295,341,171	0.60	52,921,969	1	14.81	311.0	43.2
2015-05-31T18:44:05.396	295,403,751	0.59	52,060,362	1	14.81	270.2	43.2
2015-06-01T06:03:05.396	295,444,491	0.59	51,499,475	0	14.81	243.6	43.2
2015-06-02T01:28:05.397	295,514,391	0.59	50,536,706	1	14.80	198.0	43.2
2015-06-02T18:12:05.398	295,574,631	0.59	49,706,277	0	14.79	158.7	43.2
2015-06-03T04:28:05.398	295,611,591	0.60	49,196,435	0	14.79	134.6	43.2
2015-06-06T01:13:05.401	295,859,091	0.59	45,782,381	1	14.84	333.2	43.2
2015-06-08T01:23:05.404	296,032,491	0.59	43,394,767	1	14.84	220.0	43.2
2015-06-10T01:17:05.406	296,204,931	0.59	41,017,026	1	14.83	107.5	43.2
2015-06-12T01:04:06.408	296,376,951	0.59	38,643,881	0	14.88	355.3	43.1
2015-06-16T19:05:06.414	296,787,411	0.59	32,987,485	0	14.87	87.5	43.2
2015-06-17T05:55:06.414	296,826,411	0.59	32,449,251	1	14.88	62.1	43.2
2015-06-18T19:38:06.415	296,962,191	0.60	30,577,044	0	14.93	333.5	43.1
2015-06-19T08:04:06.416	297,006,951	0.59	29,960,601	1	14.94	304.4	43.1
2015-06-20T01:00:06.416	297,067,911	0.60	29,121,357	0	14.94	264.6	43.2
2015-06-21T05:56:06.418	297,172,071	0.59	27,686,928	1	14.91	196.6	43.2
2015-06-22T00:34:06.418	297,239,151	0.59	26,762,162	0	14.90	152.8	43.2
2015-06-23T03:11:06.419	297,334,971	0.59	25,439,989	1	14.91	90.3	43.2
2015-06-27T04:58:54.923	297,687,041	0.59	20,587,098	1	14.97	220.7	43.2
2015-06-28T09:26:55.425	297,789,521	0.59	19,174,697	0	14.94	153.8	43.2
2015-06-29T04:21:55.425	297,857,621	0.59	18,236,363	1	14.94	109.3	43.2
2015-07-01T17:19:55.428	298,077,102	0.59	15,209,335	1	15.06	326.3	43.1
2015-07-02T17:48:45.429	298,165,232	0.59	13,995,915	0	15.07	268.8	43.1
2015-07-03T04:03:55.430	298,202,142	0.59	13,486,480	1	15.06	244.7	43.2

mission's approach phase, which began on 15th January 2015 (Young et al., 2008). However, because of its relatively limited spatial resolution it wasn't until later that MVIC began observing the Pluto system: the first MVIC image of Pluto and Charon was obtained on 9th April 2015, from a distance of ~115,000,000 km. From that time observations of both targets were made by MVIC regularly, often every day or every other day. During this time the sub-solar latitude increased only very slightly, from 51.2 °N to 51.5 °N. All of the observations taken by MVIC's color filters are used in this work until those taken after 3rd of July 2015 when the disk of Charon becomes well resolved so the use of aperture photometry is no longer appropriate. The results are also given for a subset of the observations. New Horizons approached the Pluto-system rapidly (Stern et al., 2015); from April to July 2015 it had decreased its distance to Charon by ~half. Thus the later observations (considered to be 29th May 2015 to 3rd July 2015) offer much higher signal-to-noise, but of course fewer total observations. The details of all the images used in this work are given in Table 1.

The observations used in this work are restricted to that of Charon with MVIC's color filters. This is because more observations were taken with the color, rather than panchromatic filters and the MVIC color Pluto light curves are described by Ennico et al. (2016). IAU standards were adopted for latitude and longitude (i.e. the right hand rule was adopted and that Charon longitudes are zero at the sub-Pluto meridian (imaged by the spacecraft on encounter day) and decrease with local time increase).

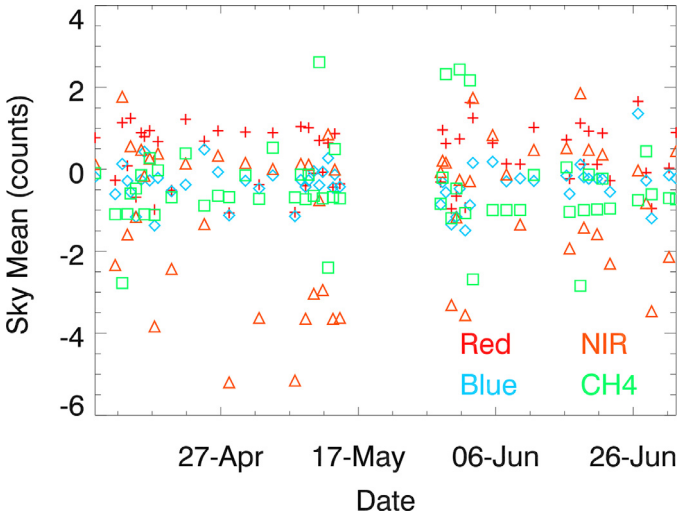

Fig. 2. The mean sky value in all the MVIC color images, derived from values inside an annulus close to Charon but not including Pluto or hot pixels. No systematic trends are observed and there are no singular erroneous points, implying that the assumed sky annulus is reasonable. The standard deviation error of these observations is smaller than the size of the symbols used. The Red, Blue, NIR and CH4 channels are depicted as red crosses, blue diamonds, orange triangles and green squares respectively. (For interpretation of the references to colour in this figure legend, the reader is referred to the web version of this article.)

2. Method and results

2.1. Data reduction and calibration

All of the MVIC observations used here were bias subtracted, which makes it possible to have small negative count rates in the image. Each of the observations was visually inspected to ensure their quality and to determine preliminary center values for Pluto and Charon. From these values the pixel separation of the two bodies was determined, which was used to set the sky annulus values. For observations with a target separation of less than 10 pixels, a sky annulus between 10 and 20 pixels from the center of Charon was assumed. Similarly if the target separation was between 10 and 15 pixels an annulus of 15 to 25 pixels was assumed. This pattern of assuming a 10 pixel wide annulus starting at the closest multiple of 5 pixels above the target separation value was continued until the target distance reached 35 pixels. At these larger separation values the distance between Charon and Pluto was so great that a sky annulus centered on Charon that fell between Charon and Pluto could be used, so an annulus of 10 to 20 pixels was once again assumed. The Charon radius and the position of the sky annulus was manually checked for each observation and tweaked when required, for example on the occasions when the sky annulus fell outside of the area of the image or there was a hot pixel inside the annulus. In these instances either the width of the annulus or the starting pixel number was decreased to provide an annulus away from the target, covered by the image that only includes dark sky. Fig. 2 gives the mean sky values derived from these annuli, it shows no trends or values notably different from the others, which implies the annuli assumed for each of the images are reasonable.

Finally for each observation the phase angle and sub-spacecraft longitude and latitude were calculated using Navigation and Ancillary Information Facility's SPICE kernels and routines (Acton, 1996; Steffl et al., 2007); these values are also given in Table 1. A basemap of Charon, showing the region observed by the MVIC observations is given in Fig. 1. Note, as Fig. 1 shows because the sub-solar latitude is ~51.3°N and the sub-spacecraft latitude is ~41.2°N not all of Charon's observed disk was illuminated (latitudes below ~38.7 °S are in darkness). The region observed by Buie et al. (2010) is also shown in the same figure for comparison.

2.2. Light curve production

The IDL routine basphote, written by Buie (Buie, 2015), was used to perform the aperture photometry for light curve construction. A detector gain of 58.6 electrons/DN was assumed (Reuter et al., 2008), and the exposure time used was directly read from each image's header. The preliminary location of Charon, its radius and the details of the sky annulus provided to the routine were as previously described. Basphote then refines the target center and outputs the target's total flux (counts/second). A secondary IDL aperture photometry routine called aper (Landsman, 1993) was used to validate the results, and the results were found to be consistent. The total flux was then calibrated using the radiometric keyword "PCHARON" as provided by the New Horizons project. The keyword is defined for each different filter, and assumes a Charon-like emission for a point source. Full details on the derivation of this keyword can be found in Howett et al. (2016).

The radiometrically-calibrated fluxes were then adjusted to account for the different distances at which they were obtained. All the observations were corrected to an arbitrary distance of 100,000,000 km. Finally, following the method of Buie et al. (2010) the results were fitted by a 2-term Fourier fit and a weighted mean. A summary of the resulting light curves for all the MVIC color filters is given in Fig. 3, and the Fourier coefficients required to fit the data are given in Table 2. The same light curves are also shown for a subset of observations obtained between 29th May 2015 and 3rd July 2015, they are shown separately in Fig. 3 for comparison.

2.3. Correction of the light curve using Hapke parameters

The various observations used to produce the light curves produced in this work were all taken within 0.5° of solar phase angle of one another (Table 1), and well away from the opposition surge that occurs close to 0° (Buie et al., 2010). So no strong phase correction is strictly required to interpret these results. However, to

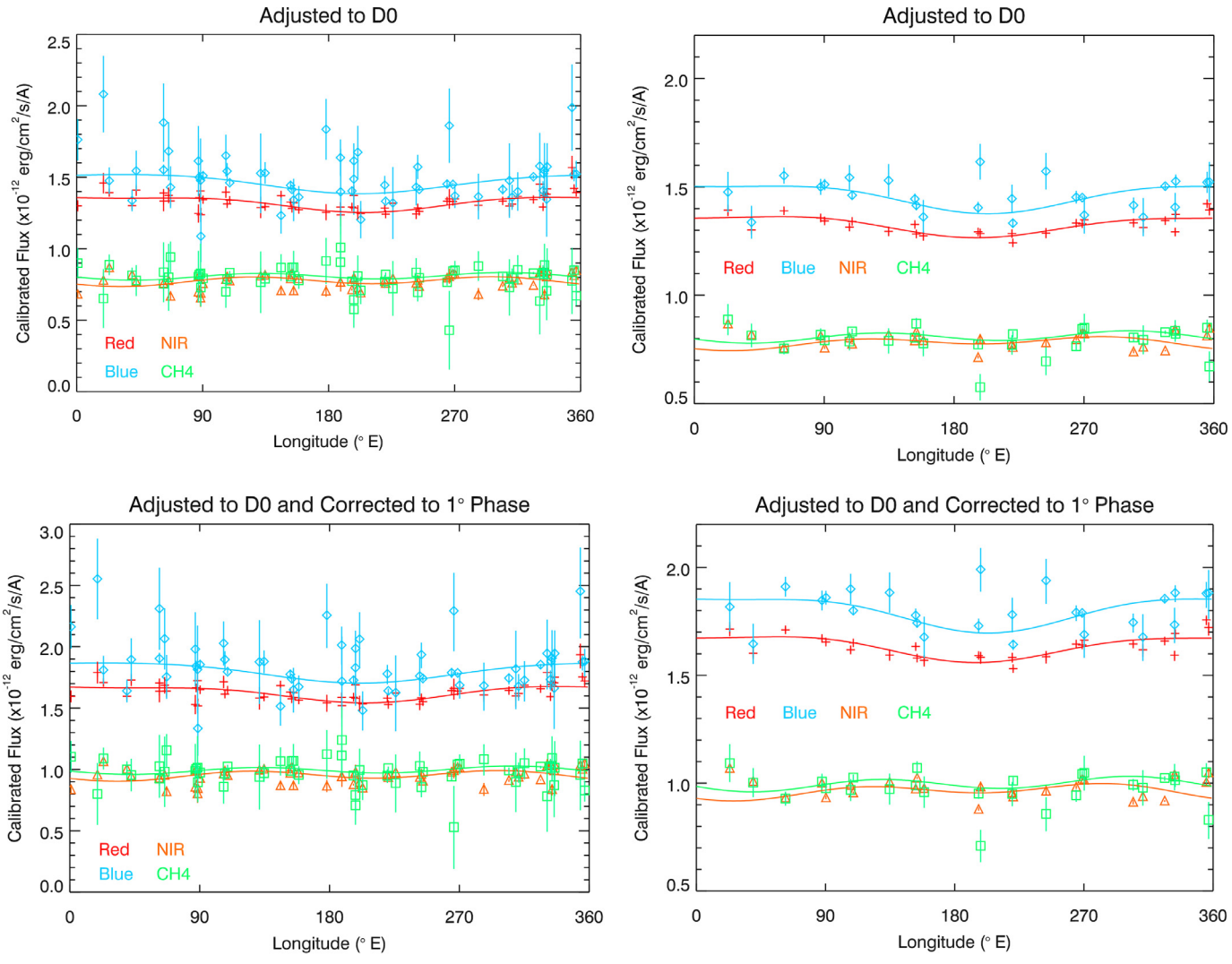

(a) Observations from 9th April to 3rd July 2015

(b) Observations from 29th May to 3rd July 2015

Fig. 3. Light curves for (a) all observations from 9th April to 3rd July (b) and a subset of this data, taken between 29th May to 3rd July, since data taken closer to encounter have a higher signal-to-noise. All observations are detailed in Table 1. For each observation period: (Top) The light curves of Charon as observed by all four of MVIC's color filters on approach to the Pluto system. The values have been radiometrically calibrated and adjusted to a distance D0, 100 million kilometers. The red crosses, blue diamonds, orange triangles and green squares show the flux observed by MVIC's red, blue, NIR and CH4 filters respectively. The lines show the Fourier curve fit to the points of a corresponding color. (Bottom) The same light curves as shown in the top figure, but now corrected to 1° phase angle. The phase changes only varies by 0.56° (14.50° to 15.06°) across the full observation period (0.28° over the subset) and is well away from the opposition surge that occurs at low phase angles, the correction factor required to bring these observations to the expected flux at 1° is therefore very similar between all observations (0.815 to 0.810). (For interpretation of the references to colour in this figure legend, the reader is referred to the web version of this article.)

follow the precedent of the community and to allow easier comparison with previous result (e.g. Buie et al., 2010) we also show results corrected to 1° phase. To do this previously derived Hapke parameters (comparable to those in Buie et al., 2010) were used to calculate a phase curve of Charon (Verbiscer, personal communication). The correction factor required varied from ~18.5% to 19.0% increase in the flux across the full observation set. Fig. 3 shows these calibrated and phase corrected light curves for all the observations, and just the late subset ones.

3. Discussion

During New Horizons' approach phase it became apparent that MVIC's NIR channel was producing spurious results. A full description of this problem, along with the workaround used for the NIR Pluto observations is given in Howett et al. (2016). It was concluded that gain drift was occurring on observations read out through electronics side 1. As Table 1 shows observations of Charon were made using both sides of the electronics. Fig. 4 shows the observed fluxes for all the MVIC filters split by electronic read out side, including the 2-term Fourier fit to those data. The same figure also shows the same fits to the subset of data used in Fig. 3, i.e. those obtained during the final few weeks of approach (29th May and 3rd of July). The light curves of all the filters (except the NIR, which is discussed further below) show the same trends in the non-subset and subset data figures, but the latter is clearer.

Unlike the other three filters, the fluxes observed using the NIR channel for a given Charon longitude have a large offset depending upon which electronic side was used to take the data, an effect particularly noticeable when the data is shown as a subset. This strongly implies that gain drift was affecting the NIR results. As such, we only use and discuss NIR observations obtained on side 0.

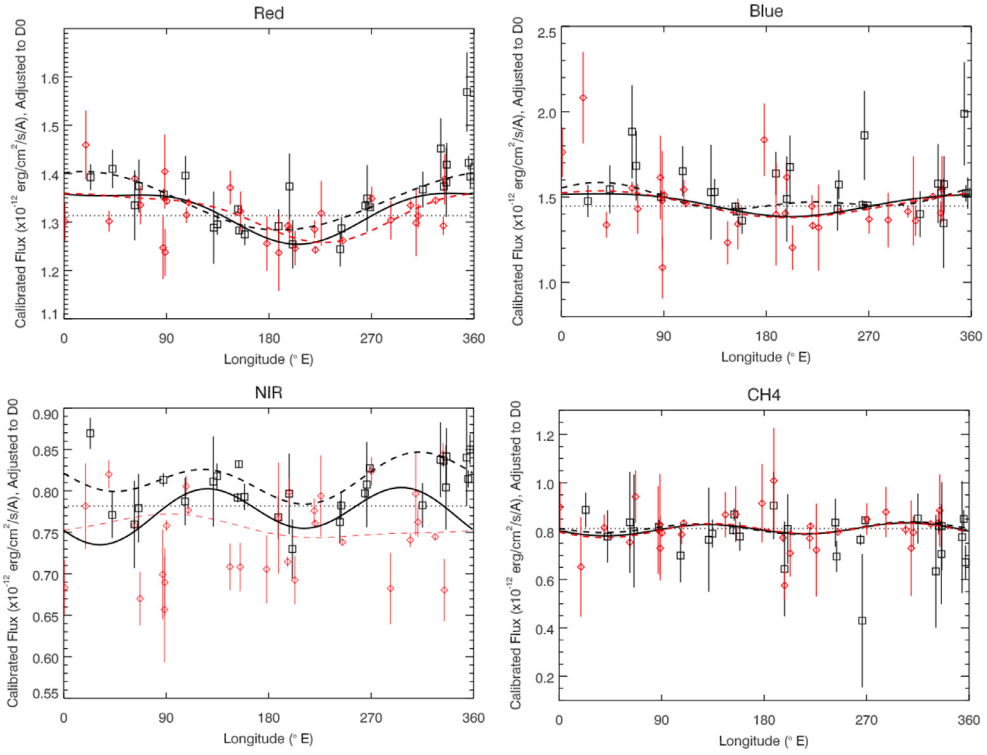

(a) Observations from 9th April to 3rd July 2015

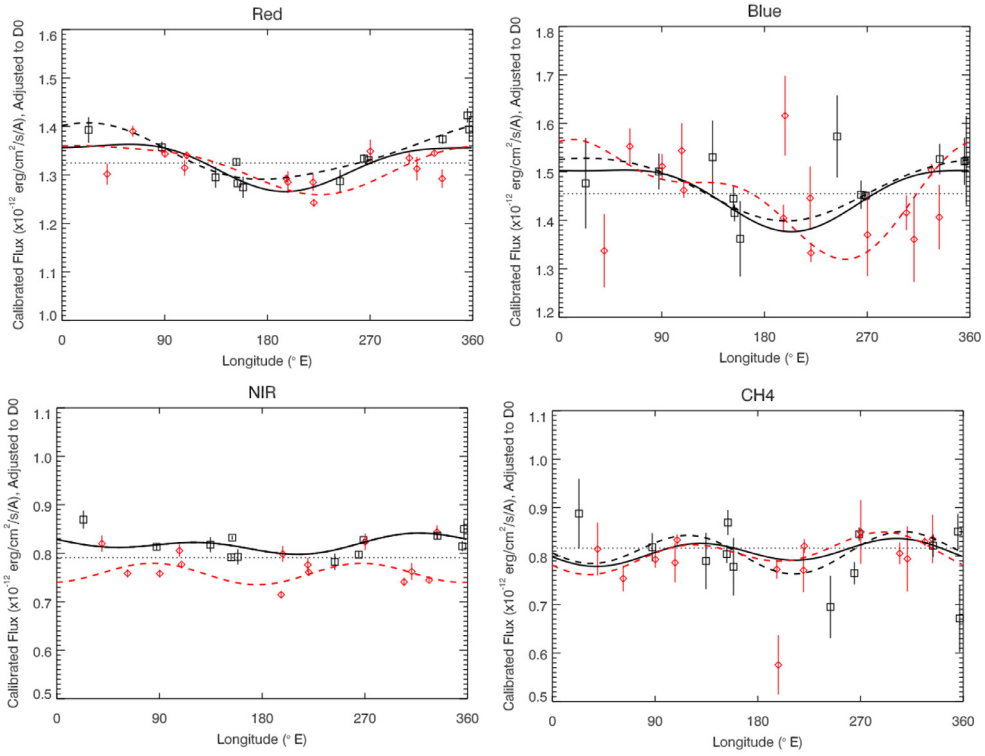

(b) Observations from 29th May to 3rd July 2015

Fig. 4. Charon light curves as determined by each of the different MVIC color filters, for (a) the full observation period: 9th April to 3rd July 2015, (b) a subset of the observations obtained from 29th May to 3rd July 2015. The red diamonds and the black squares show the results taken on electronics side 1 and side 0 respectively. The solid line shows the Fourier fit to all the data points, where as the red and black dashed line gives the fit to just side 1 and side 0 respectively. The dotted black line indicates the weighted mean of the all the observed fluxes, with the exception of NIR where only those obtained using side 0 of the electronics are used. (For interpretation of the references to colour in this figure legend, the reader is referred to the web version of this article.)

Table 2
Two-term Fourier fit to the fluxes of Charon as observed by MVIC's four color channels (x10^{-12}), given for observations taken on both electronics sides, and side 0 and side 1 only.

n	Fourier Terms (All electronics sides)				Fourier Terms (Electronics Side 0)				Fourier Terms (Electronics Side 1)			
	a	σ	b	σ	a	σ	b	σ	a	σ	b	σ
Red												
0	1.3221	0.0020			1.3439	0.0043			1.3184	0.0025		
1	0.0461	0.0030	0.0200	0.0024	0.0588	0.0052	0.0136	0.0053	0.0356	0.0049	0.0319	0.0032
2	−0.0107	0.0024	−0.0142	0.0029	−0.0009	0.0056	0.0018	0.0089	0.0041	0.0039	−0.0129	0.0041
Blue												
0	1.4629	0.0064			1.4890	0.0147			1.4587	0.0080		
1	0.0609	0.0096	0.0268	0.0075	0.0528	0.0170	0.0250	0.0171	0.0699	0.0161	0.0334	0.0104
2	−0.0090	0.0075	−0.0067	0.0092	0.0111	0.0189	0.0374	0.0312	−0.0047	0.0123	0.0029	0.0136
NIR												
0	0.7739	0.0015			0.8142	0.0030			0.7554	0.0019		
1	−0.0081	0.0022	−0.0058	0.0018	0.0125	0.0037	−0.0036	0.0037	0.0017	0.0037	0.0124	0.0025
2	−0.0132	0.0018	-0.0257	0.0021	−0.0055	0.0039	−0.0211	0.0064	−0.0043	0.0030	−0.0017	0.0031
CH4												
0	0.8077	0.0047			0.8123	0.0119			0.8066	0.0056		
1	−0.0011	0.0078	−0.0054	0.0059	0.0056	0.0142	−0.0015	0.0141	−0.0055	0.0115	−0.0064	0.0072
2	−0.0051	0.0064	−0.0223	0.0073	−0.0068	0.0156	−0.0208	0.0246	−0.0047	0.0087	−0.0251	0.0097

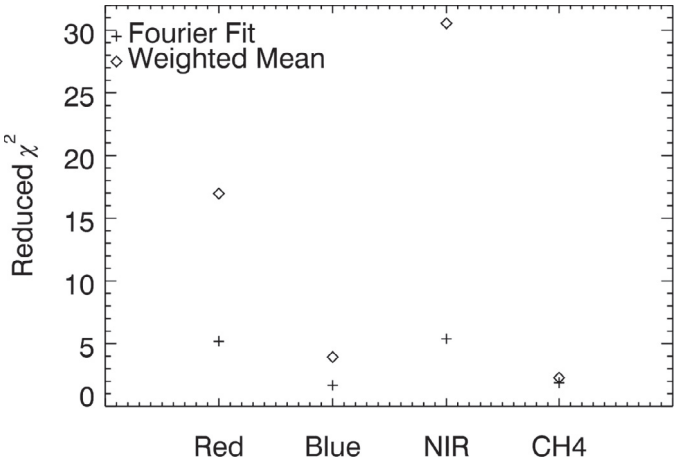

Fig. 5. Comparison of the reduced χ^2 produced by the best Fourier fit to the Charon fluxes determined from the highest signal-to-noise data (obtained between 29th May and 3rd July 2015), to that of the weighted mean of the same fluxes (except for NIR, where only those taken on electronics side 0 are considered). The Fourier fit provides a significantly better fit to the data in all but the CH4 filter, where it is only slightly better.

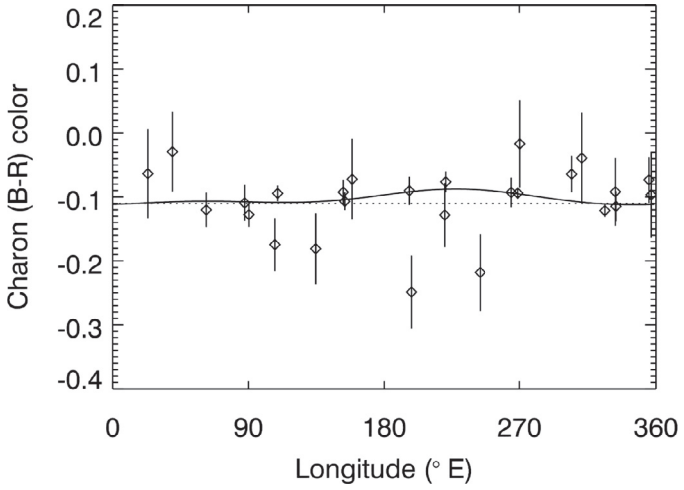

Fig. 6. Magnitude of Charon's MVIC (Blue – Red) color using data obtained after 29th May 2015. The points show magnitude difference observed between the Blue and Red MVIC channels, whilst the solid line shows the difference in the Fourier fit and the dotted line gives the weighted mean fit. The results are given at the their original phase. (For interpretation of the references to colour in this figure legend, the reader is referred to the web version of this article.)

Fig. 5 shows the reduced-χ^2 fit of the Fourier terms and the weighted mean for the subset of data obtained between the 29th May and 3rd of July. It shows that in all channels the Fourier fit provides a much better fit to the data than the weighted mean, except in the CH4 channel where the two fit almost equally well. Thus we conclude no discernable color differences are observed across Charon in the CH4 channel. It should be noted the Fourier fit doesn't produce a reduced-χ^2 fit less than 1 for the non-CH4 filters; thus the Fourier fit could be improved upon but is used here to remain consistent with literature precedents.

Charon's NIR light curve appears to have a similar shape to that of the CH4 one, with two peaks on the leading and trailing hemispheres. The CH4 channel actually lies within the NIR one (860-910 nm, and 780-975 nm respectively) so the fact that they display the same trend strengthens this result, as it was likely they'd display a similar trend. However, as discussed the CH4 fit is no better than the weighted mean so it provides a weak validation. While it is believed only the NIR side 1 of the electronics is erroneous, and those given here are for side 0, the results from this filter should be treated with some caution.

The Red and Blue MVIC filters have a higher signal-to-noise and a Fourier fit that is much better than the weighted mean (Fig. 5). They both display a similar trend: a single peak on the Pluto-facing hemisphere. This gross trend of Charon being brighter on the Pluto-facing hemisphere (centered on 180° E) is consistent with both of the previous studies of Charon's light curve (Buie et al. 1997b, 2010). The decrease in calibrated and distance corrected flux observed between the peak and the trough, assuming the full data set, is 21% and 48% in the Red and Blue channels respectively. However, it is better to compare the differences in these channels once they have been converted to magnitudes, since that is how they are presented in the literature. This is achieved simply using: $m = -2.5log_{10}(I)$ where m is the magnitude and I is the flux. Fig. 6 gives the difference in the Blue and Red values, it shows the Blue-Red light curve is approximately flat with a small maxima around 227° E. This is different to that of Buie et al. (2010) for B-V color, which displayed a double peak light curve with maxima at 150° E and 325° E, and minima at 60° E and 240° E. However, the amplitude of the Buie maxima and minima are small

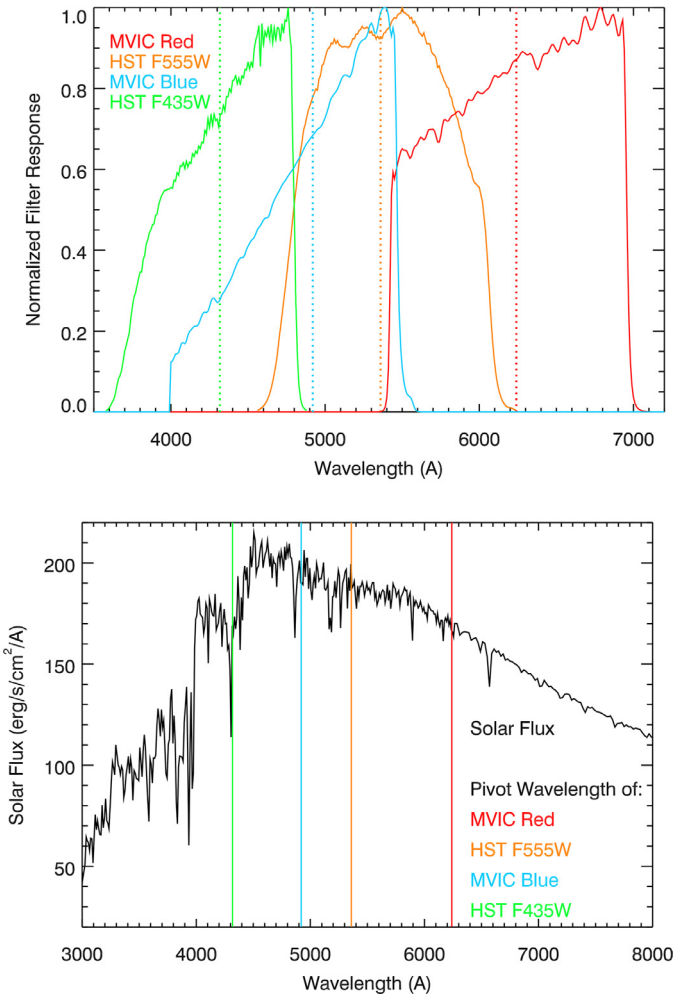

Fig. 7. A comparison of the MVIC Red and Blue filter responses with that of the HST F555W (Johnson V) and F435W (Johnson B). Top: The response of the MVIC Red, MVIC Blue, HST F555W and HST F435W filters, the dotted lines in corresponding colors show the pivot wavelength of the filters. Bottom: The pivot wavelengths of the MVIC Red and Blue filters and the HST F555W and F435W filters compared to the absolute flux solar reference spectrum from Colina et al. (1996). It shows the response of the MVIC Red/HST 555 W and MVIC Blue/F435W probe very different parts of the solar spectrum. (For interpretation of the references to colour in this figure legend, the reader is referred to the web version of this article.)

(<1% color change with longitude), which is consistent with the flat light curve found here. It is possible that the (Blue-Red) and (B-V) colors agree within the error however small differences would not be surprising as the filters probe different wavelength regions (as detailed below).

Whilst these gross trends appear consistent with literature values a more detailed comparison between the MVIC light curves and past telescopic studies cannot directly be made because the filter responses of the instruments used are very different. Buie et al. (2010) used observations made with two filters on the Hubble Space Telescope's (HST) Advanced Camera for Surveys High-resolution Camera (ACS): F435W filter (Johnson Blue) and F555W (Johnson V). It should be noted that whilst Buie et al. (2010) used the F555W filter, Buie et al. (1997b) used the F439W instead of the F435W filters. However, since the Buie et al. (2010) is considered to be an update on Buie et al. (1997b) the difference between F435W and F555W and the MVIC filters are concentrated upon.

Fig. 7 compares the MVIC filter responses (Howett et al., 2016) with that of the HST (Sirianni et al., 2005). They show not only that the responses are very different, but also that the region of they solar spectrum they probe is very different too. Fig. 7c shows for a neutral reflector the HST derived (B-V) difference at the pivot wavelength will be negative, whereas the MVIC derived (Blue-Red) difference will be net positive.

4. Conclusion

For completeness light curves of all of MVIC's four-color channels have been derived, but only two have been discussed in detail, because the CH4 channel is very noisy (primarily due to its smaller bandwidth than the other channels giving it a lower S/N) and the NIR channel may be erroneous. However, the Red and Blue channels provide light curves that have gross trends that are in good agreement with those in the literature, specifically Charon is shown to have a darker anti-Pluto hemisphere. The reason for this hemispheric difference is not known, although several methods to brighten Charon's Pluto-facing hemisphere have been postulated. These include surface processing of Charon's Pluto-facing hemisphere by thermal Pluto-shine, or the preferential deposition of bright volatiles, which have escaped Pluto, onto this region (Buie et al., 2010; Grundy et al. 2016). It is hoped further analysis of data returned by New Horizons will explain these differences.

Acknowledgement

This work was supported by NASA's New Horizons Project.

References

Acton, C.H., 1996. Ancillary data services of NASA's navigation and ancillary information facility. Planet. Space Sci. 44, 65–70.
Binzel, R.P., 1988. Hemispherical color differences on Pluto and Charon. Science 241, 1070–1072.
Binzel, R.P., Hubbard, W.B., 1997. In: Tholen, D.J., Stern, S.A. (Eds.), Pluto and Charon. Univ. Arizona Press, Tucson, AZ.
Bosh, A.S., Young, L.A., Elliot, J.L., Hammel, H.B., Baron, R.L., 1992. Photometric variability of Charon at 2.2 microns. Icarus 95, 319–324.
Buie, M.W., Tholen, A.J., Horne, K., 1992. Albedo maps of pluto and charon: initial mutual event results. Icarus 97, 211–227.
Buie, M.W., Young, E.F., Binzel, R.P., 1997a. Surface appearance of Pluto and Charon. In: Stern, S.A., Tholen, D.J. (Eds.), Pluto and Charon. Univ. Arizona Press, Tucson, pp. 269–293.
Buie, M.W., Tholen, D.J., Wasserman, L.H., 1997b. Separate lightcuves of Pluto and Charon. Icarus 25, 233–244.
Buie, M.W., Grundy, W.M., Young, E.F., Young, L.A., Stern, S.A., 2010. Pluto and Charon with hubble space telescope. 1. Monitoring global change and improved surface properties from light curves. Astron. J. 139, 1117–1127.
Buie, M.W.. General purpose IDL functions and procedures.
Christy, J.W., Harrington, R.S., 1978. The satellite of Pluto. Astron. J. 83, 1005–1008.
Cruikshank, D.P., Roush, T.L., Moore, J.M., et al., 1997. The surfaces of Pluto and Charon. In: Stern, S.A., Tholen, D.J. (Eds.), Pluto and Charon. Univ. Arizona Press, Tucson, pp. 221–267.
Colina, L., Bohlin, R.C., Castelli, F., 1996. The 0.12-2.5 micron absolute flux distribution of the Sun for comparison with solar analog stars. Astron. J. 112, 307–316.
Ennico, K., Howett, C.J.A., Parker, A.H., Olkin, C.B., Reuter, D.C., Grundy, W.M, Throop, A.H.B., Buie, M.W., Porter, S.B., Weaver, H.A., Young, L.A., Stern, S.A., Beyer, R.A., Binzel, R.P., Buratti, B.J., Cheng, A.F., Cook, J.C., Cruikshank, D.P., Dalle Ore, C.M., Earle, A.M., Jennings, D.E., Linscott, I.R., Lunsford, A.W., Parker, J.Wm., Phillippe, S., Protopapa, S., Quirico, E., Schenk, P.M., Schmitt, B., Singer, K.N., Spencer, J.R., Stansberry, J.A., Tsang, C.C.C., Weigle II, G.E., Verbiscer, A.J., 2016. Pluto's light curves, as observed by New Horizons' MVIC camera on approach to the Pluto system. Icarus In Preparation.
Grundy, W.M., Cruikshank, D.P., Gladstone, G.R., Howett, C.J.A., Lauer, T.R., Spencer, J.R., Summers, M.E., Buie, M.W., Earle, A.M., Ennico, K., Parker, J.Wm., Porter, S.B., Singer, K.N., Stern, S.A., Verbiscer, A.J., Beyer, R.A., Binzel, R.P., Buratti, B.J., Cook, J.C., Dalle Ore, C.M., Olkin, C.B., Parker, A.H., Protopapa, S., Quirico, E., Retherford, K.D., Robbins, S.J., Schmitt, B., Stansberry, J., Umurhan, O.M., Weaver, H.A., Young, L.A., Zangari, A.M., Bray, V., Cheng, A.F., McKinnon, W.B., McNutt, R.L., Moore, J.M., Reuter, D.C., Schenk, P.M., the New Horizons Science Team, 2016. Formation of Charon's red polar caps. Nature doi:10.1038/nature19340.
Hansen, C.J., Paige, D.A, 1996. Seasonal nitrogen cycles on Pluto. Icarus 120, 247.

Howett, C.J.A., Parker, A.H., Olkin, C.B., Reuter, D.C., Ennico, K., Grundy, W.M, Graps, A.L., Harrison, K.P., Throop, H.B., Buie, M.W., Lovering, J.R., Porter, S.B., Weaver, H.A., Young, L.A., Stern, S.A., Beyer, R.A., Binzel, R.P., Buratti, B.J., Cheng, A.F., Cook, J.C., Cruikshank, D.P., Dalle Ore, C.M., Earle, A.M., Jennings, D.E., Linscott, I.R., Lunsford, A.W., Parker, J.Wm., Phillippe, S., Protopapa, S., Quirico, E., Schenk, P.M., Schmitt, B., Singer, K.N., Spencer, J.R., Stansberry, J.A., Tsang, C.C.C., Weigle II, G.E., Verbiscer, A.J., 2016. Inflight radiometric calibration of new horizons' multispectral visible imaging camera (MVIC). Icarus Submitted.

Landsman, W.B., 1993. The IDL astronomy user's library. In: Hanisch, R.J., Brissenden, R.J.V., Barnes, J. (Eds.), Astronomical Data Analysis Software and Systems II, A.S.P. Conference Series, 52, p. 246.

Reuter, D.C., Stern, S.A., Scherrer, J., Jennings, D.E., Baer, J., Hanley, J., Hardaway, L., Lunsford, A., McMuldroch, S., Moore, J., Olkin, C., Parizek, R., Reitsma, H., Sabatke, D., Spencer, J., Stone, J., Throop, H., Van Cleve, J., Weigle, G.W., Young, L.A., 2008. Ralph: a visible/infrared imager for the new horizons pluto/kuiper belt mission. Space Sci. Rev. 140, 129–154.

Reinsch, K., Burwitz, V., Festou, M.C., 1994. Albedo maps of Pluto and improved physical parameters of the Pluto-Charon system. Icarus 108, 209–218.

Sirianni, M., Jee, M.J., Benítez, N., Blakeslee, J.P., Martel, A.R., Meurer, G., Clampin, M., De Marchi, G., Ford, H.C., Gilliland, R., Hartig, G.F., Illingworth, G.D., Mack, J., McCann, W.J., 2005. The photometric performance and calibration of the hubble space telescope advanced camera for surveys. Pub. Astron. Soc. Pacific 117, 1049–1112.

Steffl, A.J., Peterson, J., Carcich, B., Nguyen, L., Stern, S.A., 2007. New Horizons SPICE kernels v1.0. NASA Planetary Data System NH-J/P/SS-SPICE-6-V1.0.

Stern, S.A., Bagenal, F., Ennico, K., Gladstone, G.R., Grundy, W.M., McKinnon, W.B., Moore, J.M., Olkin, C.B., Spencer, J.R., Weaver, H.A., Young, L.A., Andert, T., Andrews, J., Banks, M., Bauer, B., Bauman, J., Barnouin, O.S., Bedini, P., Beisser, K., Beyer, R.A., Bhaskaran, S., Binzel, R.P., Birath, E., Bird, M., Bogan, D.J., Bowman, A., Bray, V.J., Brozovic, M., Bryan, C., Buckley, M.R., Buie, M.W., Buratti, B.J., Bushman, S.S., Calloway, A., Carcich, B., Cheng, A.F., Conard, S., Conrad, C.A., Cook, J.C., Cruikshank, D.P., Custodio, O.S., Dalle Ore, C.M., Deboy, C., Dischner, Z.J.B., Dumont, P., Earle, A.M., Elliott, H.A., Ercol, J., Ernst, C.M., Finley, T., Flanigan, S.H., Fountain, G., Freeze, M.J., Greathouse, T., Green, J.L., Guo, Y., Hahn, M., Hamilton, D.P., Hamilton, S.A., Hanley, J., Harch, A., Hart, H.M., Hersman, C.B., Hill, A., Hill, M.E., Hinson, D.P., Holdridge, M.E., Horanyi, M., Howard, A.D., Howett, C.J.A., Jackman, C., Jacobson, R.A., Jennings, D.E., Kammer, J.A., Kang, H.K., Kaufmann, D.E., Kollmann, P., Krimigis, S.M., Kusnierkiewicz, D., Lauer, T.R., Lee, J.E., Lindstrom, K.L., Linscott, I.R., Lisse, C.M., Lunsford, A.W., Mallder, V.A., Martin, N., McComas, D.J., McNutt Jr., R.L., Mehoke, D., Mehoke, T., Melin, E.D., Mutchler, M., Nelson, D., Nimmo, F., Nunez, J.I., Ocampo, A., Owen, W.M., Paetzold, M., Page, B., Parker, A.H., Parker, J.W., Pelletier, F., Peterson, J., Pinkine, N., Piquette, M., Porter, S.B., Protopapa, S., Redfern, J., Reitsema, H.J., Reuter, D.C., Roberts, J.H., Robbins, S.J., Rogers, G., Rose, D., Runyon, K., Retherford, K.D., Ryschkewitsch, M.G., Schenk, P., Schindhelm, E., Sepan, B., Showalter, M.R., Singer, K.N., Soluri, M., Stanbridge, D., Steffl, A.J., Strobel, D.F., Stryk, T., Summers, M.E., Szalay, J.R., Tapley, M., Taylor, A., Taylor, H., Throop, H.B., Tsang, C.C.C., Tyler, G.L., Umurhan, O.M., Verbiscer, A.J., Versteeg, M.H., Vincent, M., Webbert, R., Weidner, S., Weigle II, G.E., White, O.L., Whittenburg, K., Williams, B.G., Williams, S., Woods, W.W., Zangari, A.M., Zirnstein, E., 2015. The Pluto system: initial results from its exploration by new horizons. Science 350, 292–301.

Young, L.E., Stern, S.A., Weaver, H.A., Bagenal, F., Binzel, R.P., Buratti, B., Cheng, A.F., Cruikshank, D., Gladstone, G.R., Grundy, W.M., Hinson, D.P., Horanyi, M., Jennings, D.E., Linscott, I.R., McComas, D.J., McKinnon, W.B., McNutt, R., Moore, J.M., Murchie, S., Olkin, C.B., Porco, C.C., Reitsema, H., Reuter, D.C., Spencer, J.R., Slater, D.C., Strobel, D., Summers, M.E., Tyler, G.L., 2008. New horizons: anticipated scientific investigations at the Pluto system. Space Sci. Rev. 140, 93–127.